1,2-Bis(pyridine-2-carboxamido)benzenate(2−), $(bpb)^{2-}$: A Noninnocent Ligand. Syntheses, Structures, and Mechanisms of Formation of $[(n\text{-}Bu)_4N][Fe^{IV}_2(\mu\text{-}N)(bpb)_2(X)_2]$ ($X = CN^-$, N_3^-) and the Electronic Structures of $[M^{III}(bpb^{ox1})(CN)_2]$ (M = Co, Fe)

Sujit K. Dutta, Udo Beckmann, Eckhard Bill, Thomas Weyhermüller, and Karl Wieghardt*

Max-Planck-Institut für Strahlenchemie, D-45470 Mülheim an der Ruhr, Germany

Received February 3, 2000

The well-known tetradentate ligand 1,2-bis(pyridine-2-carboxamido)benzenate(2−), $(bpb)^{2-}$, and its 4,5-dichloro analogue, $(bpc)^{2-}$, are shown to be "noninnocent" ligands in the sense that in coordination compounds they can exist in their radical one- and diamagnetic two-electron-oxidized forms $(bpb^{ox1})^-$ and $(bpb^{ox2})^0$ (and $(bpc^{ox1})^-$ and $(bpc^{ox2})^0$), respectively. Photolysis of high-spin $[(n\text{-}Bu)_4N][Fe^{III}(bpb)(N_3)_2]$ and its $(bpc)^{2-}$ analogue in acetone solution at room temperature generates the diamagnetic dinuclear complex $[(n\text{-}Bu)_4N][Fe^{IV}_2(\mu\text{-}N)(bpb)_2(N_3)_2]$ and its $(bpc)^{2-}$ analogue; the corresponding cyano complex $[(n\text{-}Bu)_4N][Fe^{IV}_2(\mu\text{-}N)(bpb)_2(CN)_2]$ has been prepared via N_3^- substitution by CN^-. Photolysis in frozen acetonitrile solution produces a low-spin ferric species ($S = {}^1/_2$) which presumably is $[Fe^{III}(bpb^{ox2})(N)(N_3)]^-$, as has been established by EPR and Mössbauer spectroscopy. The mononuclear complexes $[(n\text{-}Bu)_4N][Fe^{III}(bpb)(CN_2)]$ (low spin), $[Et_4N][Co^{III}(bpb)(CN)_2]$ and $Na[Co^{III}(bpc)(CN)_2]\cdot 3CH_3OH$ can be electrochemically or chemically one-electron-oxidized to give $[Fe^{III}(bpb^{ox1})(CN)_2]^0$ ($S = 0$), $[Co^{III}(bpb^{ox1})(CN)_2]^0$ ($S = {}^1/_2$), and $[Co^{III}(bpc^{ox1})(CN)_2]^0$ ($S = {}^1/_2$). All complexes have been characterized by UV−vis, EPR, and Mössbauer spectroscopy, and their electro- and magnetochemistries have been studied. The crystal structures of $[(n\text{-}Bu)_4N][Fe^{III}(bpb)(N_3)_2]\cdot {}^1/_2C_6H_5CH_3$, $Na[Fe^{III}(bpb)(CN)_2]$, $Na[Co^{III}(bpc)(CN)_2]\cdot 3CH_3OH$, $[(n\text{-}Bu)_4N][Fe^{IV}_2(\mu\text{-}N)(bpb)_2(CN)_2]$, and $[(n\text{-}Bu)_4N][Fe^{IV}_2(\mu\text{-}N)(bpb)(N_3)_2]$ have been determined by single-crystal X-ray diffraction.

Introduction

In a series of photolysis experiments at ambient temperature, we recently showed that low-spin *trans*-$[Fe^{III}(cyclam)(N_3)_2]ClO_4$ in acetonitrile produces the mixed-valent $Fe^{III}Fe^{IV}$ dinuclear species $[\{trans\text{-}(cyclam)Fe(N_3)\}_2(\mu\text{-}N)]^{2+}$ with an $S_t = {}^1/_2$ ground state (cyclam = 1,4,8,11-tetraazacyclotetradecane).[1] Mössbauer spectroscopy unequivocally demonstrated that the valences are localized on an intermediate-spin ferric ion ($S = {}^3/_2$) and a low-spin Fe^{IV} ion ($S = 1$). Photolysis at cryogenic temperatures (<80 K) in frozen solutions allowed us to identify the mononuclear precursors *trans*-$[Fe^V(N)(cyclam)(N_3)]^+$ and $[Fe^{II}(cycam)(N_3)]^+$, which, upon annealing to 150 K, form in a bimolecular reaction the $Fe^{III}{-}N{-}Fe^{IV}$ species. These Fe^V and Fe^{II} precursors are the primary photolysis products as shown in eq 1. Similarly, photolysis of high-spin $[LFe^{III}(L')(N_3)]^{n+}$, where

$$Fe^{III}\text{-}N_3 \begin{array}{l} \xrightarrow{h\bullet\nu} Fe^V{\equiv}N + N_2 \\ \xrightarrow{h\bullet\nu} Fe^{II} \quad + N_3^\bullet \;(\rightarrow N_2) \end{array} \qquad (1)$$

L represents 1,4,7-trimethyl-1,4,7-triazacyclononane and L′ is a bidentate catecholate dianion ($n = 0$) or acetylacetonate monoanion ($n = 1$), produces mixed-valent (μ-nitrido)diiron species $[\{L(L')Fe\}_2(\mu\text{-}N)]^{0/+}$ which contain also a $[Fe^{III}(\mu\text{-}N)\text{-}Fe^{IV}]^{4+}$ core but with an $S_t = {}^3/_2$ ground state.[2] Again, Mössbauer spectroscopy established that the valences are localized. Some of these species can be chemically one-electron-oxidized to the corresponding dinuclear Fe^{IV}_2 species. The diamagnetic complexes $[\{L(Cl_4cat)Fe^{IV}\}_2(\mu\text{-}N)]Br$ and $[\{L(nadiol)Fe^{IV}\}_2(\mu\text{-}N)]PF_6$ have been characterized by X-ray crystallography.[2]

Photolyses of azido(porphinato)iron(III)[3] (or the corresponding phthalocyaninato[4]) complexes have been shown to also produce mixed-valent but *delocalized* species such as $[\{(tpp)\text{-}Fe^{3.5}\}_2(\mu\text{-}N)]$ ($S_t = {}^1/_2$).[3] Here also, the primary formation of $Fe^V{\equiv}N$ and ferrous species has been invoked to rationalize the observed product distribution.[5]

Collins et al.[6,7] have shown that redox-inert macrocyclic tetraamido-*N* ligands are capable of stabilizing unusual high-valent transition metal ions such as cobalt(IV)[6] and iron(IV).[7] Therefore, we felt that, by using azidoiron(III) complexes containing robust ligands derived from 1,2-bis(pyridine-2-carboxamido)benzene and 4,5-dichloro-1,2-bis(pyridine-2-carboxamido)benzene[8] ($H_2(bpb)$ and $H_2(bpc)$), shown in Chart 1, it might be possible to generate and characterize neutral $[N{\equiv}Fe^V\text{-}$

(1) Meyer, K.; Bill, E.; Mienert, B.; Weyhermüller, T.; Wieghardt, K. *J. Am. Chem. Soc.* **1999**, *121*, 4859.

(2) (a) Jüstel, T.; Weyhermüller, T.; Wieghardt, K.; Bill, E.; Lengen, M.; Trautwein, A. X.; Hildebrandt, P. *Angew. Chem., Int. Ed. Engl.* **1995**, *34*, 669. (b) Jüstel, T.; Müller, M.; Weyhermüller, T.; Kressl, C.; Bill, E.; Hildebrandt, P.; Lengen, M.; Grodzicki, M.; Trautwein, A. X.; Nuber, B.; Wieghardt, K. *Chem.*−*Eur. J.* **1999**, *5*, 793.

(3) (a) Summerville, D. A.; Cohen, I. A. *J. Am. Chem. Soc.* **1976**, *98*, 1747. (b) Buchler, J. W.; Dreher, C. *Z. Naturforsch., B* ***1984***, *39B*, 222.

(4) Goedken, V. L.; Ercolani, C. *J. Chem. Soc., Chem. Commun.* **1984**, 378.

(5) Wagner, W.-D.; Nakamoto, K. *J. Am. Chem. Soc.* **1989**, *111*, 1590.

(6) (a) Collins, T. J.; Uffelman, E. S. *Angew. Chem., Int. Ed. Engl.* **1989**, *28*, 1509. (b) Collins, T. J.; Powell, R. D.; Slebodnick, C.; Uffelman, E. S. *J. Am. Chem. Soc.* **1990**, *112*, 899.

(7) Kostka, K. L.; Fox, B. G.; Hendrich, M. P.; Collins, T. J.; Rickard, C. E. F.; Wright, L. J.; Münck, E. *J. Am. Chem. Soc.* **1993**, *115*, 6746.

10.1021/ic0001107 CCC: $19.00
Published on Web 06/24/2000

Chart 1

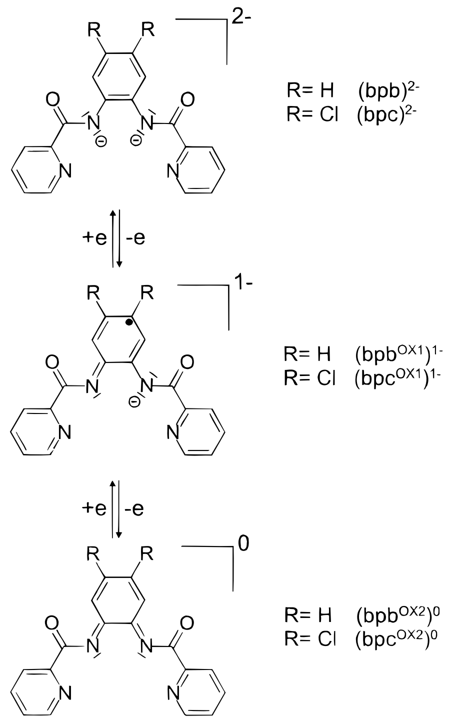

Chart 2

Complexes	
$[Fe^{III}(bpb)Cl(H_2O)]\cdot H_2O$	**1**
$[Fe^{III}(bpc)Cl(H_2O)]\cdot H_2O$	**1a**
$[(C_4H_9)_4N][Fe^{III}(bpb)(N_3)_2]\cdot 0.5C_6H_5CH_3$	**2**
$[(C_4H_9)_4N][Fe^{III}(bpc)(N_3)_2]\cdot 0.5C_6H_5CH_3$	**2a**
$Na[Fe^{III}(bpb)(CN)_2]$	**3**
$[(C_4H_9)_4N][Fe^{III}(bpb)(CN)_2]$	**3′**
$[Fe^{III}(bpb^{OX1})(CN)_2]$	**4**
$[(C_2H_5)_4N][Co^{III}(bpb)(CN)_2]$	**5**
$Na[Co^{III}(bpc)(CN)_2]\cdot 3CH_3OH$	**5a**
$[(C_4H_9)_4N][Fe^{IV}_2(\mu\text{-}N)(bpb)_2(CN)_2]$	**6**
$[(C_4H_9)_4N][Fe^{IV}_2(\mu\text{-}N)(bpb)_2(N_3)_2]$	**7**
$[(C_4H_9)_4N][Fe^{IV}_2(\mu\text{-}N)(bpc)_2(N_3)_2]$	**7a**

(bpb)] and [N≡Fe^{V}(bpc)] species. This hope was fueled by the fact that [N≡Cr^{V}(bpb)] is a stable species, which has been characterized by X-ray crystallography.[9]

Indeed, we found that photolysis of high-spin $[Fe^{III}(bpb)(N_3)_2]^-$ [10] and $[Fe^{III}(bpc)(N_3)_2]^-$ in solution at 20 °C produced the diamagnetic species $[\{Fe^{IV}(bpb)X\}_2(\mu\text{-}N)]^-$ and $[\{Fe^{IV}(bpc)X\}_2(\mu\text{-}N)]^-$ ($X = CN^-$, N_3^-) in >60% yield. However, the putative intermediates [N≡Fe^{V}(bpb)] and [N≡Fe^{V} (bpc)] could not be detected at cryogenic temperatures (<80 K). Instead, ligand oxidation to (bpb^{ox2}) or (bpc^{ox2}) (Chart 1) had to be invoked.[11,12] To firmly establish the noninnocence of the ligands, we prepared the mononuclear complexes shown in Chart 2, investigated their spectroelectrochemistry, and characterized their one- and two-electron-oxidized forms by EPR and Mössbauer spectroscopy. Che et al.[11] have previously postulated and given some spectroelectrochemical evidence that the coordinated (bpb)$^{2-}$ ((bpc)$^{2-}$) ligand undergoes two successive one-electron, ligand-centered oxidation steps, with formation of (bpb^{ox1})$^-$ and (bpb^{ox2})^0 ((bpc^{ox1})$^-$ and (bpc^{ox2})^0). Note that the monoanions (bpb^{ox1})$^-$ and (bpc^{ox1})$^-$ are organic radicals ($S = {}^1/_2$) whereas the corresponding dianions are diamagnetic ($S = 0$).

Experimental Section

The ligand compounds 1,2-bis(pyridine-2-carboxamido)benzene, H_2(bpb), and 4,5-dichloro-1,2-bis(pyridine-2-carboxamido)benzene, H_2(bpc), were prepared according to literature procedures.[8]

[Fe^{III}(bpb)Cl(H$_2$O)]·H$_2$O (1). H_2(bpb) (0.32 g; 1.0 mmol) and NaOH (0.08 g; 2.0 mmol) were added to a stirred solution of $FeCl_3\cdot 6H_2O$ (0.27 g; 1.0 mmol) in CH_3OH (40 mL). After the mixture was refluxed for 3 h, the dark green microcrystals that had precipitated were collected by filtration, washed with methanol, and air-dried. Yield: 0.31 g (70%). Anal. Calcd for $[C_{18}H_{14}N_4O_3ClFe]\cdot H_2O$: C, 48.71; H, 3.61; N, 12.63; Fe, 12.59. Found: C, 48.5; H, 3.6; N, 12.4; Fe, 12.3.

[Fe^{III}(bpc)Cl(H$_2$O)]·H$_2$O (1a). This complex was synthesized similarly to $[Fe^{III}(bpb)Cl(H_2O)]$ in ref 13. By following the above procedure for the prepartion of **1** but using H_2(bpc) instead of H_2(bpb), we obtained green crystals of $[Fe^{III}(bpc)Cl(H_2O)]\cdot H_2O$ (**1a**).

[(*n*-Bu)$_4$N][Fe^{III}(bpb)(N$_3$)$_2$]·0.5C$_6$H$_5$CH$_3$ (2). A preparation for $[Et_4N][Fe^{III}(bpb)(N_3)_2]$ was described in ref 10. Better yields were obtained by following the procedure described here. To an acetone suspension (40 mL) of **1** (0.44 g; 1.0 mmol) were added excess NaN_3 (0.65 g; 10 mmol) and tetrabutylammonium chloride (0.28 g; 1.0 mmol), and the mixture was refluxed for 3 h. From the resulting deep green solution excess NaN_3 was filtered off, and the filtrate was evaporated to dryness by rotary evaporation. The oily residue was dissolved in a minimum of CH_3CN (~10 mL), and toluene (40 mL) was added. Standing overnight at 0 °C produced green crystals of **2**. Yield: 0.56 g (75%). Anal. Calcd for $[C_{34}H_{48}N_{11}O_2Fe]\cdot 0.5C_6H_5CH_3$: C, 60.49; H, 6.99; N, 20.70; Fe, 7.50. Found: C, 60.2; H, 7.1; N, 20.3; Fe, 7.6.

[(*n*-Bu)$_4$N][Fe^{III}(bpc)(N$_3$)$_2$]·0.5C$_6$H$_5$CH$_3$ (2a). This compound was prepared as described above for **2** by using **1a** as the starting material. Yield: 0.57 g (70%). Anal. Calcd for $[C_{34}H_{46}N_{11}O_2Cl_2Fe]\cdot 0.5C_6H_5CH_3$: C, 55.36; H, 6.15; N, 18.94; Fe, 6.87. Found: C, 55.2; H, 6.4; N, 19.1; Fe, 7.1.

Na[Fe^{III}(bpb)(CN)$_2$] (3).[10] A methanol suspension (50 mL) of **1** (0.42 g; 1.0 mmol) and excess NaCN (0.7 g) was stirred at ambient temperature for about 3 h until the appearance of a clear green solution from which green crystals slowly precipitated. Single crystals suitable for X-ray crystallography were obtained by slow recrystallization of this material from a CH_3CN solution. Yield: 0.29 g (65%). Anal. Calcd for $C_{20}H_{12}N_6O_2NaFe$: C, 53.70; H, 2.68; N, 18.79; Fe, 12.59. Found: C, 53.5; H, 2.65; N, 18.5; Fe, 12.7. The previously reported physical properties[10] are in excellent agreement with those found here (IR, EPR, μ_{eff}).

[(*n*-Bu)$_4$N][Fe^{III}(bpb)(CN)$_2$] (3′). This salt was obtained in 80% yield as green microcrystals from a CH_3CN solution of **3** to which an excess of $[(n\text{-}Bu)_4N]Cl$ had been added.

[Fe^{III}(bpb^{ox1})(CN)$_2$] (4). This complex was isolated from a dry, argon-purged acetonitrile solution (40 mL) of **3′** (25 mg) containing 0.10 M $[(n\text{-}Bu)_4N]PF_6$ in a coulometry cell. Electrolysis at a constant potential of +0.8 V vs Fc$^+$/Fc at a platinum net working electrode produced brown microcrystals of **4**, which were collected by filtration, washed with CH_3CN, and air-dried. Yield: 14.5 mg (90%). The same species may be obtained chemically by reaction of **3′**

(8) Barnes, D. J.; Chapman, R. L.; Vagg, R. S.; Watton, E. C. *J. Chem. Eng. Data* **1978**, *23*, 349.
(9) (a) Che, C.-M.; Ma, J.-X.; Wong, W.-T.; Lai, T.-F.; Poon, C.-K. *Inorg. Chem.* **1988**, *27*, 2547. (b) Azuma, N.; Ozawa, T.; Tsuboyama, S. *J. Chem. Soc., Dalton Trans.* **1994**, 2609.
(10) Ray, M.; Mukherjee, R.; Richardson, J. F.; Buchanan, R. M. *J. Chem. Soc., Dalton Trans.* **1993**, 2451.
(11) Mak, S.-T.; Wong, W.-T.; Yam, V. W.-W.; Lai, T.-F.; Che, C.-M. *J. Chem. Soc., Dalton Trans.* **1991**, 1915.
(12) Che, C.-M.; Leung, W.-H.; Li, C.-K.; Cheng, H.-Y.; Peng, S.-M. *Inorg. Chim. Acta* **1992**, *196*, 43.
(13) Patra, A. K.; Mukherjee, R. *Polyhedron* **1999**, *18*, 1317.

Table 1. Crystallographic Data

	2	**3**	**5a**	**6**	**7**
empirical formula	$C_{37.5}H_{52}FeN_{11}O_2$	$C_{20}H_{12}FeN_6NaO_2$	$C_{23}H_{22}Cl_2CoN_6NaO_5$	$C_{54}H_{60}Fe_2N_{12}O_4$	$C_{52}H_{60}Fe_2N_{16}O_4$
fw	744.75	447.20	615.29	1052.84	1084.86
space group	$Pna2_1$	$P2_1/n$	$P2_1/c$	$P2_1/n$	$P\bar{1}$
a, Å	15.946(3)	8.942(1)	8.176(1)	13.176(2)	9.4431(7)
b, Å	15.685(3)	14.111(2)	17.006(2)	17.145(3)	13.9919(9)
c, Å	30.523(5)	15.707(2)	19.286(2)	23.102(4)	20.4449(14)
α, deg	90	90	90	90	77.19(2)
β, deg	90	102.53(2)	97.88(2)	103.91(2)	85.91(2)
γ, deg	90	90	90	90	74.43(2)
V, Å^3	7634(2)	1934.7(4)	2656.2(5)	5066(2)	2537.2(3)
Z	8	4	4	4	2
T, K	100(2)	100(2)	100(2)	100(2)	100(2)
ρ_{calcd}, g cm^{-3}	1.296	1.535	1.539	1.380	1.420
diffractometer used	Nonius Kappa CCD	Siemens SMART	Siemens SMART	Siemens SMART	Nonius Kappa CCD
no. of data	59 702	13 807	16 361	20 993	38 431
no. of unique data^a	7613	4322	2089	5505	7600
no. of params	923	271	327	652	667
μ(Mo Kα), cm^{-1}	4.44	8.32	9.10	6.32	6.35
R1^{a,b}	0.0526	0.0320	0.0742	0.0609	0.0442
wR2^{a,c}	0.1161	0.0833	0.1630	0.1706	0.0966

^{a} Observation criterion: $I > 2\sigma(I)$. ^{b} $R1 = \sum||F_o| - |F_c||/\sum|F_o|$. ^{c} $wR2 = \{\sum[w(F_o^2 - F_c^2)^2]/\sum[w(F_o^2)^2]\}^{1/2}$; $w = 1/\sigma^2(F_o^2) + (aP)^2 + bP$; $P = (F_o^2 + 2F_c^2)/3$. ^{d} Radiation: Mo Kα; $\lambda = 0.710\ 73$ Å.

dissolved in CH_3CN with 1 equiv of $[Ni^{III}(tacn)_2](ClO_4)_3$ (tacn = 1,4,7-triazacyclononane).[14] Anal. Calcd for $C_{20}H_{12}N_6O_2Fe$: C, 56.62; H, 2.83; N, 19.81; Fe, 13.17. Found: C, 56.4; H, 2.9; N, 19.7; Fe, 13.2.

$[Et_4N][Co^{III}(bpb)(CN)_2]$ (5). To a solution of $[Co^{II}(bpb)]\cdot H_2O$[11,15] (0.20 g; 0.50 mmol) in CH_3OH (20 mL) was added dropwise at 50 °C a methanol (10 mL) solution of KCN (0.10 g; 1.5 mmol). After 30 min of stirring in the presence of air at 20 °C, CH_2Cl_2 (50 mL) was added. The solution was cooled at 0 °C for 2 h, after which the precipitated excess KCN was removed by filtration and the reaction volume was reduced to 20 mL by evaporation. Standing overnight at ambient temperature produced a deep red precipitate of $K[Co(bpb)(CN)_2]$, which was collected by filtration and added to a solution of CH_3OH (20 mL) and $[Et_4N]Cl$ (50 mg), leading to the crystallization of **5**. Yield: 95 mg. Anal. Calcd for $C_{28}H_{32}N_7O_2Co$: C, 60.32; H, 5.78; N, 17.59; Co, 10.57. Found: C, 60.1; H, 5.6; N, 17.4; Co, 10.3. ^{1}H NMR (400 MHz, CD_3OD), δ: = 9.27 (d, ^3J = 5.5 Hz, 2H); 8.75 (BB′ part, 2H); 8.29 (ddd, ^3J = 7.7 Hz, 7.7 Hz, ^4J = 1.4 Hz, 2H); 8.11 (d, ^3J = 7.9 Hz, 2H); 7.86 (ddd, ^3J = 5.7 Hz, 7.5 Hz, ^4J = 1.7 Hz, 2H); 7.09 (AA′ part, 2H); 3.27 (q, 8H); 1.28 (t, 12H). $Na[Co(bpb)(CN)_2]$ has been described in the literature.[11]

$Na[Co^{III}(bpc)(CN)_2]\cdot 3CH_3OH$ (5a). Slow recrystallization of $Na[Co^{III}(bpc)(CN)_2]$[11] from CH_3OH produced red crystals of **5a** that were suitable for X-ray crystallography. Anal. Calcd for $C_{23}H_{22}N_6O_5Cl_2CoNa$: C, 44.90; H, 3.60; N, 13.66; Co, 9.58. Found: C, 44.5; H, 3.5; N, 13.5; Co, 9.4. ^{1}H NMR (250 MHz, CD_3OD), δ: = 9.26 (d, ^3J = 5.4 Hz, 2H); 8.84 (s, 2H); 8.30 (ddd, ^3J = 7.7 Hz, 7.7 Hz, ^4J = 1.4 Hz, 2H); 8.11 (dd, ^3J = 7.8 Hz, ^4J = 1.6 Hz, 2H); 7.88 (ddd, ^3J = 5.7 Hz, 7.5 Hz, ^4J = 1.6 Hz).

$[(n\text{-}Bu)_4N][Fe^{IV}_2(\mu\text{-}N)(bpb)_2(CN)_2]$ (6). A dry CH_3CN solution (100 mL) of **2** (0.7 g; 1.0 mmol) in a quartz photolysis apparatus was purged with argon for 15 min and irradiated at ambient temperature with an HPK lamp (250 nm) for 4 h. The deep green color of the original solution changed to red-brown when the reaction was complete. The reaction volume was reduced by evaporation with an argon flow for 2 days. The red crystals that precipitated were collected by filtration and dried in vacuo. This residue consisted of **6** (85%) and $[(n\text{-}Bu)_4N][Fe^{IV}_2(\mu\text{-}N)(bpb)_2(N_3)_2]$ (**7**) (15%). To a CH_3CN solution of this mixture were added excess NaCN (0.4 g) and $[(n\text{-}Bu)_4N]Cl$ (0.28 g). After 4 h of stirring at 20 °C, excess NaCN was filtered off and the reaction volume was reduced to 10 mL by rotary evaporation. Red-brown crystals of pure **6** were obtained. Yield: 0.31 g (60%). Anal. Calcd for $C_{54}H_{60}N_{12}O_4Fe$: C, 61.61; H, 5.70; N, 15.97; Fe, 10.62. Found: C, 61.5; H, 5.75; N, 16.0; Fe, 10.7.

(14) Wieghardt, K.; Walz, W.; Nuber, B.; Weiss, J.; Ozarowski, A.; Stratemeier, H.; Reinen, D. *Inorg. Chem.* **1986**, *25*, 1650.

$[(n\text{-}Bu)_4N][Fe^{IV}_2(\mu\text{-}N)(bpb)_2(N_3)_2]$ (7). This complex was prepared as described above for **6** except that the photolysis was performed in dry acetone. The crude red-brown material obtained was recrystallized from a CH_3CN/toluene mixture (1:1). Yield: 0.16 g (60%). Anal. Calcd for $C_{52}H_{60}N_{16}O_4Fe_2$: C, 57.58; H, 5.53; N, 20.66; Fe, 10.30. Found: C, 57.4; H, 5.3; N, 20.7; Fe, 10.2.

$[(n\text{-}Bu)_4N][Fe^{IV}_2(\mu\text{-}N)(bpc)_2(N_3)_2]$ (7a). This compound was prepared as described above for **7** by using dry acetone as the solvent and complex **2a** as the starting material. Yield: 0.20 g (65%). Anal. Calcd for $C_{52}H_{56}N_{16}O_4Cl_2Fe_2$: C, 51.07; H, 4.58; N, 18.33; Fe, 9.14. Found: C, 51.2; H, 4.7; N, 18.1; Fe, 9.0.

Photolyses at 77 K. Complex **2** (30 mmol) was dissolved in 2.5 mL of dry, argon-purged acetone. This solution was added dropwise (slowly!) to a beaker containing liquid dinitrogen, whereupon the droplets froze. The frozen solution was photolyzed using a 185−419 nm light source (Rayonet reactor, model RPR-100, equipped with 16 tubes for light) for 3 h under liquid nitrogen. One part of the frozen solution was then taken for Mössbauer and the other for EPR spectroscopic measurements at cryogenic temperatures.

X-ray Crystallographic Data Collection and Refinement of the Structures. Dark red single crystals of **2**, **3**, and **6** and orange single crystals of **5a** and **7** were picked directly from the mother liquors with glass fibers and each was fixed with a drop of perfluoropolyether. The crystals were immediately mounted on diffractometers, each equipped with a cryogenic nitrogen cold stream to prevent loss of solvent of crystallization. Crystallographic data for the compounds and diffractometers used are listed in Table 1. Cell constants in each case were obtained from a least-squares fit of a subset of more than 1500 strong reflections. Intensity data were collected at −100(2) °C by taking frames at 0.3° (Siemens SMART) and 0.5° (Nonius Kappa) in ω. Data were corrected for Lorentz and polarization effects. Semiempirical absorption corrections for **3**, **5a**, and **6** were carried out with the program SADABS.[16] Intensities of **7** were corrected for absorption using the Gaussian face-indexed method. The Siemens ShelXTL[17] software package (Version 5) was used for the solution and refinement of the structures and for producing the ORTEP diagrams. All structures were solved and refined by direct methods and difference Fourier techniques. Neutral-atom scattering factors incorporated in the program were used. All non-hydrogen atoms were refined anisotropically except for the carbon atom of one methyl group in the $[(n\text{-}Bu)_4N]^+$ cation of **7**, which

(15) Chapman, R. L.; Vagg, R. S. *Inorg. Chim. Acta* **1979**, *33*, 227.
(16) Sheldrick, G. M. *SADABS*; Universität Göttingen: Göttingen, Germany, 1994.
(17) *ShelXTL*, V.5; Siemens Analytical X-ray Instruments, Inc.: Madison, WI, 1994.

was found to be disordered over three sites. A split-atom model with occupancies of 0.5:0.25:0.25 and isotropic temperature factors was used here. All hydrogen atoms were placed at calculated positions and refined as riding atoms with isotropic displacement parameters.

Physical Measurements. Infrared spectra (400−4000 cm^{-1}) of solid samples in KBr disks were recorded on a Perkin-Elmer 2000 FT-IR/FT-NIR spectrometer. Cyclic voltammetric and coulometric measurements were performed on EG&G equipment (model 273A potentiostat/galvanostat) for acetonitrile solutions of the samples containing 0.10 M [N(*n*-Bu)$_4$]PF$_6$ as supporting electrolyte. UV−vis spectra of solutions were recorded on a Perkin-Elmer Lambda 19 spectrophotometer in the range 200−1600 nm. Temperature-dependent magnetic susceptibilities of powdered samples were measured by using a SQUID magnetometer (Quantum Design) at 1.0 T (2.0−300 K). Corrections for underlying diamagnetism were made by using tabulated Pascal constants. X-band EPR spectra were recorded on a Bruker ESP 300E spectrometer equipped with a helium flow cryostat (Oxford Instruments ESR 910). Mössbauer data were obtained on an alternating constant-acceleration spectrometer. The minimum experimental line width was 0.24 mm s^{-1} (full width at half-height). The sample temperature was maintained constant either in an Oxford Instruments Variox or an Oxford Instruments Mössbauer-Spectromag 2000 cryostat. The latter is a split-pair superconducting magnet system for applied fields up to 8 T, where the temperatures of samples can be varied in the range 1.5−250 K. The field at the samples was oriented perpendicular to the γ-beam. The ^{57}Co/Rh source (1.8 GBq) was positioned at room temperature inside the gap of the magnet system at a zero-field position. Isomer shifts are quoted relative to iron metal at 300 K. Low-temperature EPR and magnetic Mössbauer spectra were analyzed on the basis of a spin-Hamiltonian description of the electronic ground-state spin multiplet, either $H_e = \mu_B \mathbf{B}\cdot g\cdot \mathbf{S}$ for the low-spin ferric system ($S = {}^1/_2$) or $H_e = D[S_z^2 - S(S+1)/3 + (E/D)(S_x^2 - S_y^2)] + \mu_B \mathbf{B}(\bar{g}\cdot\mathbf{S} + \bar{g}'\cdot\mathbf{S}') - 2(\mathbf{S}\cdot\bar{J}\cdot\mathbf{S}')$ for the spin-coupling interpretation of photolyzed **2** with $S = 1$ and $S' = {}^1/_2$, where D and E/D are the axial and rhombic zero-field parameters of Fe(IV) and $\bar{J} = J^{iso}\cdot\bar{1} + \bar{J}^{aniso}$ (where J^{iso} and $\bar{J}^{aniso}$ are the isotropic and anisotropic exchange coupling parameters). The Mössbauer hyperfine spectra were calculated by using the usual nuclear Hamiltonian. EPR simulations for $S = {}^1/_2$ systems in fluid or frozen solution were performed with the program EPR written by F. Neese (University Konstanz, 1993).

Results

Preparation of the Complexes. [Et$_4$N][Fe^{III}(bpb)(N$_3$)$_2$] ($S = {}^5/_2$) and Na[Fe^{III}(bpb)(CN)$_2$] (**3**) ($S = {}^1/_2$) were previously synthesized and characterized by UV−vis, EPR, and IR spectroscopy and solution susceptibility measurements by Mukherjee et al.[10] Some electrochemical experiments were also described. In our quest for structural and detailed spectroscopic information on these high- and low-spin species, we have synthesized the following complexes as single crystals suitable for X-ray crystallography (Chart 1). [Fe^{III}(bpb)Cl(H$_2$O)]·H$_2$O (**1**) and [Fe^{III}(bpc)Cl(H$_2$O)]·H$_2$O (**1a**)[12] were obtained from alkaline (NaOH) methanol solutions of the respective ligand complexes, H$_2$(bpb) and H$_2$(bpc), and FeCl$_3$·6H$_2$O as dark green microcrystals. The reactions of **1** and **1a** with excess sodium azide and tetra-*n*-butylammonium chloride in acetone and crystallization from CH$_3$CN/toluene (1:4) produced green crystals of [(*n*-Bu)$_4$N][Fe^{III}(bpb)(N$_3$)$_2$]·0.5tol (**2**) and [(*n*-Bu)$_4$N][Fe^{III}(bpc)(N$_3$)$_2$]·0.5tol (**2a**), respectively (tol = toluene). Similarly, the reaction of **1** in methanol with an excess of NaCN produced green single crystals of Na[Fe^{III}(bpb)(CN)$_2$] (**3**). Compound **3** was added to a solution of CH$_3$CN and [(*n*-Bu)$_4$N]Cl, producing green crystals of [(*n*-Bu)$_4$N][Fe^{III}(bpb)(CN)$_2$] (**3′**). Electrochemical oxidation of **3′** in CH$_3$CN at 0.8 V vs Fc$^+$/Fc resulted in the slow deposition of brown microcrystals of [Fe^{III}(bpb^{ox1})(CN)$_2$] (**4**). The same species was obtained from a chemical oxidation of **3′** in CH$_3$CN with 1 equiv of [Ni(tacn)$_2$](ClO$_4$)$_3$.[14]

Na[Co^{III}(bpb)(CN)$_2$] and Na[Co^{III}(bpc)(CN)$_2$] were synthesized according to the literature procedures.[11,15] We synthesized [Et$_4$N][Co^{III}(bpb)(CN)$_2$] (**5**) by metathesis because this salt is better suited for electrochemical investigations in CH$_3$CN solution. Slow recrystallization of Na[Co^{III}(bpc)(CN)$_2$] from methanol produced red single crystals of Na[Co^{III}(bpc)(CN)$_2$]·3CH$_3$OH (**5a**) suitable for X-ray crystallography.

Continuous irradiation of a solution of **2** in dry CH$_3$CN under an argon atmosphere for 4 h at ambient temperature changed the original deep green color of the starting solution to red-brown. Upon evaporation of the solvent, red microcrystals of a mixture of [(*n*-Bu)$_4$N][Fe$^{IV}_2$(μ-N)(bpb)$_2$(CN)$_2$] (**6**) (85%) and [(*n*-Bu)$_4$N][Fe$^{IV}_2$(μ-N)(bpb)$_2$(N$_3$)$_2$] (**7**) (15%) was obtained in 60% overall yield based on the starting material **2**. Complex **7** can be converted to **6** in CH$_3$CN by addition of NaCN. If the above photolysis reaction of **2** is carried out in dry acetone, **7** is the only isolable product. Similarly, photolysis of **2a** in dry acetone yields [(*n*-Bu)$_4$N][Fe$^{IV}_2$(μ-N)(bpc)$_2$(N$_3$)$_2$] (**7a**). Species **7** and **7a** can formally be envisaged as the reaction products of a nitridoiron(V) intermediate which reacts rapidly in a bimolecular fashion with the starting materials **2** and **2a**, respectively, yielding the dinuclear Fe^{IV}−N−Fe^{IV} core as is depicted in eq 2. Note that this scheme implies that photolysis of **2** and **2a**

$$[\mathrm{Fe^{III}(bpb)(N_3)_2}]^- \xrightarrow[-\mathrm{N_2}]{h\bullet\nu} \begin{array}{l}[\mathrm{Fe^{V}(N)(bpb)(N_3)}]^- \quad \text{or} \\ [\mathrm{Fe^{III}(N)(bpb^{ox2})(N_3)}]^- \\ \quad \Big\downarrow {\scriptstyle +\mathbf{2}} \atop {\scriptstyle -\mathrm{N_3^-}} \\ [\mathrm{Fe^{IV}_2(\mu\text{-}N)(bpb)_2(N_3)_2}]^- \end{array} \qquad (2)$$

proceeds *without* formation of ferrous species via homolytic Fe−N$_3$ bond cleavage. This is in contrast to the results reported previously for *trans*-[Fe^{III}(cyclam)(N$_3$)$_2$]$^+$, the photolysis product of which at ambient temperature is the mixed-valent species [(N$_3$)(cyclam)Fe^{III}(μ-N)Fe^{IV}(cyclam)(N$_3$)]$^{2+}$. This species is formed in quantitative yield via a bimolecular reaction of [Fe^V(N)(cyclam)(N$_3$)]$^+$ and [Fe^{II}(cyclam)(N$_3$)]$^+$, both of which have been identified as primary photolysis products of *trans*-[Fe^{III}(cyclam)(N$_3$)$_2$]$^+$ at 10−77 K by Mössbauer spectroscopy.[1]

The infrared spectra of solid samples of the complexes (KBr disks) display, in general, three strong bands in the range 1500−1700 cm^{-1} (Table S27 (Supporting Information)), which may be split in some instances because of crystal field effects. These bands are assigned to C═O and C−N stretching modes of the carboxamido moieties of the tetradentate ligands (bpb) and (bpc) and should be sensitive to the oxidation levels of these ligands. Indeed, all complexes in Table S27 containing (bpb)$^{2-}$ and (bpc)$^{2-}$ ligands display an intense band in the narrow range 1640−1615 cm^{-1} (ν(C═O)). Upon one-electron oxidation of **3**, generating the (bpb^{ox1})$^-$ level in **4**, this band shifts to 1695, 1681 cm^{-1}.

Crystal Structures. The crystal structures of the mononuclear complexes **2**, **3**, and **5a** and of the dinuclear species **6** and **7** have been determined by single-crystal X-ray crystallography. Figures 1 and 2 show the structures of the mono- and dinuclear anions, respectively. Table 2 summarizes selected bond distances and angles for the first coordination spheres of these complexes, and Table S26 (Supporting Information) gives C−O, C−N, and some C−C bond lengths of the coordinated ligands.

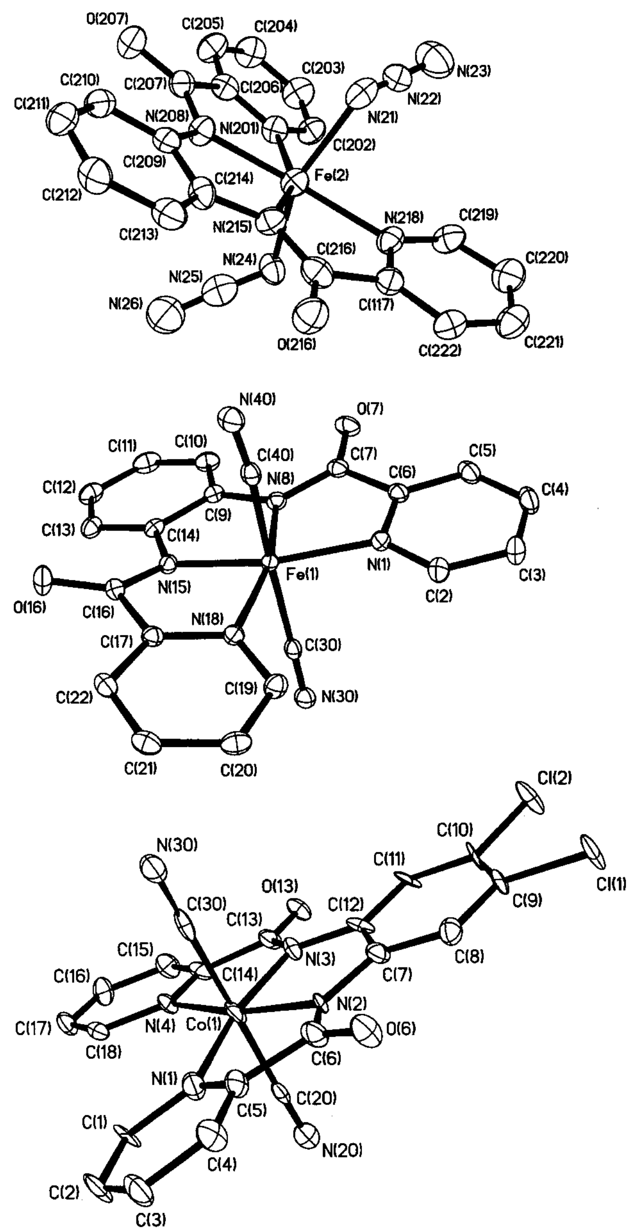

Figure 1. Structures of mononuclear complexes in crystals of **2** (top), **3** (middle), and **5a** (bottom). The thermal ellipsoids are drawn at the 40% level. H atoms are omitted for the sake of clarity.

All complexes contain an equatorially bound, tetradentate bis(carboxamido) ligand, $(bpb)^{2-}$ or $(bpc)^{2-}$. The C−O, $C_{pyridine}$−N, and $C_{carboxy}$−N distances at 1.24 ± 0.01, 1.41 ± 0.01, and 1.34 ± 0.01 Å, respectively, agree well with those reported for [N≡Cr(bpb)],[9] $[Et_4N][Fe^{III}(bpc)(CH_3CO_2)_2]\cdot CHCl_3$,[10] $[Co^{III}(bpc)(CH_2CH_2C(CH_3){=}CH_2)(H_2O)]$,[11] $[Co^{III}(bpb)Et(H_2O)]$,[11] $[Fe^{III}(bpc)(1\text{-}MeIm)_2]ClO_4$,[12] $[Fe^{III}(bpc)Cl(DMF)]$,[13] and $[Et_3HN][Fe^{III}(bpb)Cl_2]\cdot CH_3CN$.[18] These distances do not vary much with the nature of central metal ion (Cr^{V}, Co^{III}, or Fe^{III}) or the spin state (high or low spin) or the formal oxidation state of the metal ion; they are indicative of the oxidation level of the $(bpb)^{2-}$ or $(bpc)^{2-}$ ligand.

Complexes **2** and **3** contain the octahedral monoanions $[Fe^{III}(bpb)(N_3)_2]^-$ and $[Fe^{III}(bpb)(CN)_2]^-$, respectively, where the former has a high-spin and the latter a low-spin central ferric ion. This difference in spin state is clearly borne out by the differing $Fe{-}N_{pyridine}$ and $Fe{-}N_{amide}$ bond lengths, which are significantly longer for the former than for the latter. Crystals of **2** contain two crystallographically independent anions which differ only slightly in their geometrical details.

While the axial cyano ligands in **3** are nearly linearly arranged (α(C−Fe−C) = 171.7(6)°), the corresponding azido ligands in **2** are not ($\alpha(N_{azide}{-}Fe{-}N_{azide})$ = 145.6(2) and 150.9(2)° for the first and second anions, respectively). This feature appears to be electronic in nature, since all crystallographically characterized high-spin complexes $[Fe(bpp)X_2]^n$ or $[Fe(bpc)X_2]^n$ display this deviation from a regular octahedral geometry regardless of the nature of X. Thus, in $[Fe(bpc)Cl(DMF)]$,[13] $[Fe^{III}(bpb)Cl_2]^-$,[18] and $[Fe^{III}(bpc)(CH_3CO_2)_2]^-$,[10] the X−Fe−X′ angles are 145.4(2), 152.3(1), and 166.3(1)°, respectively. In contrast, for the low-spin complex $[Fe^{III}(bpc)(1\text{-}MeIm)_2]^+$, the $N_{imidazole}{-}Fe{-}N_{imidazole}$ angle is 174.9(1)°.[12]

Complex **5a** contains the octahedral monoanion $[Co^{III}(bpc)(CN)_2]^-$, sodium ions, and methanol molecules of crystallization. All Co−N bond distances are short (∼1.90−1.97 Å) and are indicative of a low-spin t_{2g}^6 configuration of the central cobalt(III) ion. The sodium ions are five-coordinate, binding to the terminal nitrogen of the cyano groups, one of the carboxamide O atoms of the ligand, and three methanol O atoms. In **3**, the sodium ions are coordinated in an intermolecular fashion to the nitrogen atoms of the cyano ligands (forming a distorted NaN_4 tetrahedron).

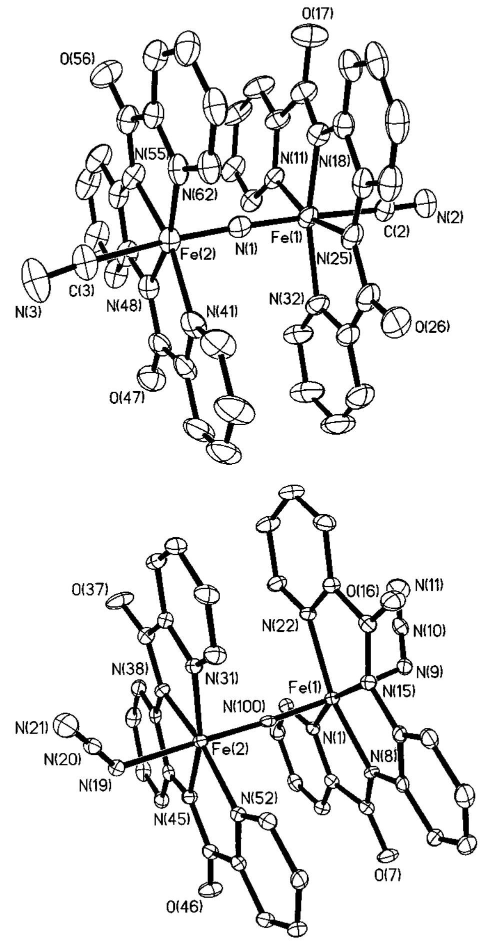

Figure 2. Structures of the dinuclear complexes containing the $[Fe^{IV}{=}N{=}Fe^{IV}]^{5+}$ core in crystals of **6** (top) and **7** (bottom). The thermal ellipsoids are drawn at the 40% level. H atoms are omitted for the sake of clarity.

(18) Yang, Y.; Diederich, F.; Valentine, J. S. *J. Am. Chem. Soc.* **1991**, *113*, 7195.

Table 2. Selected Bond Distances (Å) and Angles (deg)

Complex **2**			
Fe1−N11	2.071(5) (2.040(5))	Fe1−N118	2.184(4) (2.174(7))
Fe1−N14	2.042(6) (2.102(5))	Fe1−N115	2.072(4) (2.049(44)
N14−N15	1.072(6) (1.086(7))	Fe1−N108	2.045(4) (2.055(4))
N15−N16	1.210(8) (1.198(8))	Fe1−N(101)	2.189(5) (2.171(4))
N11−N12	1.095(7) (1.149(7))		
N12−N13	1.203(8) (1.218(8))		
N11−Fe1−N4	145.6(2) (150.9(2))		
Complex **3**			
Fe1−N1	1.997(1)	Fe1−N18	1.996(1)
Fe1−N8	1.890(1)	Fe1−C30	1.961(2)
Fe1−N15	1.895(1)	Fe1−C40	1.977(2)
C40−N40	1.152(2)	C30−N30	1.150(2)
Na−O16*	2.247(1)	Na−N30*	2.333(2)
Na−N40	2.359(1)	Na−O7	2.219(1)
C40−Fe1−C30	171.7(6)		
Complex **5a**			
Co1−N1	1.979(4)	Co1−N4	1.972(4)
Co1−N2	1.910(6)	Co1−C30	1.92(1)
Co1−N3	1.903(7)	Co1−C20	1.92(1)
C20−N20	1.17(1)	C30−N30	1.16(1)
C20−Co1−C30	176.6(4)		
Complex **6**			
Fe1−N1	1.662(4)	Fe1−N18	1.910(4)
Fe1−N25	1.912(4)	Fe1−N32	2.007(4)
Fe1−N11	2.027(3)	Fe1−C2	2.032(5)
Fe2−N1	1.656(4)	Fe2−N55	1.902(4)
Fe2−N48	1.908(4)	Fe2−N41	1.996(4)
Fe2−N62	2.012(4)	Fe2−C3	2.029(5)
N2−C2	1.147(5)	C3−N3	1.152(6)
Fe2−N1−Fe1	177.2(2)	Fe1−C2−N2	177.7(4)
Fe2−C3−N3	174.7(6)		
Complex **7**			
Fe1−N100	1.644(2)	Fe1−N22	2.007(2)
Fe1−N15	1.902(2)	Fe1−N1	2.013(2)
Fe1−N8	1.913(2)	Fe1−N9	2.060(2)
Fe2−N100	1.642(2)	Fe2−N31	2.009(2)
Fe2−N38	1.901(2)	Fe2−N52	2.023(2)
Fe2−N45	1.911(2)	Fe2−N19	2.071(2)
N9−N10	1.195(2)	N10−N11	1.165(2)
N19−N20	1.202(3)	N20−N21	1.166(3)
Fe1−N100−Fe2	176.7(1)	Fe2−N19−N20	122.6(2)
Fe1−N9−N10	120.1(1)	N100−Fe2−N19	174.0(1)
N100−Fe1−N9	173.8(1)		

Crystals of **6** and **7a** consist of the dinuclear monoanions $[\{Fe^{IV}(bpb)(CN)\}_2(\mu\text{-}N)]^-$ and $[\{Fe^{IV}(bpc)(N_3)\}_2(\mu\text{-}N)]^-$, respectively, and well-separated tetra-*n*-butylammonium cations. The $Fe-N_{amido}$ distances at 1.91 ± 0.01 Å are as short as those in low-spin **3**, 1.89 ± 0.01 Å, whereas the $Fe-N_{pyridine}$ bond lengths at 2.01 ± 0.01 Å are slightly longer but are still significantly shorter than those in high-spin **2**, 2.18 ± 0.01 Å. These data are in excellent agreement with an oxidation state of IV ($S = 1$) for the central iron ions. The bridging $Fe-N_b$ distance at 1.65 ± 0.01 Å is very short and indicative of a covalent Fe═N double bond. Other similar short distances have been reported: 1.69 ± 0.01 Å for $[\{LFe^{IV}(nadiol)\}_2(\mu\text{-}N)]PF_6$[2b] (L = 1,4,7-trimethyl-1,4,7-triazacyclononane; nadiol^{2-} = naphthalene-2,3-diolate); 1.703(1) Å for $[\{L(Cl_4cat)Fe^{IV}\}_2(\mu\text{-}N)]Br$[2a] ($Cl_4cat^{2-}$ = tetrachlorocatecholate); and 1.650(1) Å for $(PNP)_2$-$[\{Fe^{IV}(N_3)(pc)\}_2(\mu\text{-}N)]I_3{\cdot}2C_2H_5$,[19,20] which is the closest structural analogue of **7** (pc = phthalocyaninate(2−) or -(1−)). For the asymmetric complex $[(THF)(tpp)Fe^{IV}-N-Fe^{IV}(pc)(H_2)]$-$(I_5){\cdot}2THF$, the $Fe-N_b$ distances are reported as 1.65(2) and 1.63(2) Å.[21] In all cases, including **6** and **7**, the $[Fe(\mu\text{-}N)Fe]^{5+}$ structural unit is symmetric and linear. The iron ions are in an octahedral environment where the sixth coordination site, which is trans to the nitrido bridge, is occupied by weakly bound cyanide (**6**) or azide (**7**).

(19) Kienast, A.; Homborg, H. *Z. Anorg. Allg. Chem.* **1998**, *624*, 233.

Table 3. Electrochemical Data[a]

complex	redox potentials $E_{1/2}$, V vs Fc^+/Fc (ΔE_p, mV)[b]
3,**3′**	+1.20 (90) r, +0.22 (80) r, −1.19 (75) r
5	+0.90 (71) r, +0.39 (66) r
5a	+1.01 (66) r, +0.545 (64) r
6	+0.53 (95) r, +0.40 (70) r, −1.32 (300) r, −1.6 irr
7	+0.61 (110) r, +0.47 (80) r, −1.10 (75) r
7a	+0.75 irr, +0.59 irr, −0.92 (140) r, −1.08 (90) r

[a] Cyclic voltammograms were recorded in CH_3CN (0.10 M $[(n\text{-}Bu)_4N]PF_6$ supporting electrolyte; scan rate 200 mV s^{-1}) at a glassy carbon working electrode; r = reversible; irr = irreversible (peak potentials are given in these cases). [b] Peak potential difference ($E_{p,a} - E_{p,c}$); for ferrocenium/ferrocene (Fc^+/Fc), it is 85 mV.

Electronic Spectra and Magnetic Properties of the Complexes. The electronic spectra of the complexes in acetonitrile solution were recorded at 20 °C in the range 250−1000 nm; the results are summarized in Table S28 (Supporting Information). All spectra are dominated by intense ligand-based electronic transitions (250−470 nm) and ligand-to-metal charge-transfer bands in the visible region for species containing a t_{2g}^n ($n < 6$) subshell.

The magnetic properties of solid complexes were elucidated by temperature-dependent magnetic susceptibility measurements in the range 4−300 K obtained with a SQUID magnetometer. Complexes **1** and **2** each contain a high-spin ferric ion, as judged from their temperature-independent (50−300 K) magnetic moments, whereas **3** contains a low-spin ferric ion (μ_{eff}(300 K) = 2.01 μ_B). These measurements are in good agreement with the literature.[10,12,13]

Complexes **4**, **6**, and **7** have an $S = 0$ ground state; they all display substantial temperature-independent paramagnetism of ∼0.6 μ_B at 300 K which decreases to ∼0.12 μ_B at 10 K. The temperature dependence was satisfactorily fitted with χ_{TIP} values of 140 × 10^{-6} emu for **4** and 128 × 10^{-6} emu for **6** and **7**, respectively.

The cobalt(III) complexes **5** and **5a** are also diamagnetic, as judged from their ^{1}H NMR spectra (see Experimental Section).

Electro- and Spectroelectrochemistry and EPR Spectra of the Complexes. Cyclic and square-wave voltammograms of the complexes in acetonitrile solutions with 0.10 M $[(n\text{-}Bu)_4N]$-PF_6 as the supporting electrolyte were recorded at a glassy carbon working electrode. Ferrocene (Fc) was used as the internal standard, and all redox potentials are referenced to the Fc^+/Fc couple. The results are summarized in Table 3.

The octahedral dicyano complexes **3**, **3′**, **5** and **5a** each display two reversible one-electron-transfer oxidation waves in the ranges +0.2 to +0.55 V and +0.9 to +1.2 V, respectively. Figure S1 (Supporting Information) shows the cyclic voltammogram of **3**. In agreement with the results reported by Che et al.,[11] we assign these oxidation waves to the steps depicted in eq 3. These are ligand-centered processes, as we show below

(20) The complex $[\{BrFe^{IV}(pc)\}_2(\mu\text{-}N)]$ is thought to contain a phthalocyaninato(1−) radical, a diamagnetic phthalocyaninato(2−) ligand, and two Fe^{IV} ions. The $Fe-N_b$ distance is reported at 1.639(2) Å. See: Moubaraki, B.; Benlian, D.; Baldy, A.; Pierrot, M. *Acta Crystallogr.* **1989**, *C45*, 393.

(21) Ercolani, C.; Jubb, J.; Pennesi, G.; Russo, U.; Trigiante, G. *Inorg. Chem.* **1995**, *34*, 2535.

$$[M^{III}(bpb)(CN)_2]^- \underset{-e}{\overset{+e}{\leftrightarrows}} [M^{III}(bpb^{ox1})(CN)_2]^0 \underset{-e}{\overset{+e}{\leftrightarrows}} [M^{III}(bpb^{ox2})(CN)_2]^+$$

$$[M^{III}(bpc)(CN)_2]^- \underset{-e}{\overset{+e}{\leftrightarrows}} [M^{III}(bpc^{ox1})(CN)_2]^0 \underset{-e}{\overset{+e}{\leftrightarrows}} [M^{III}(bpc^{ox2})(CN)_2]^+$$

$$M = Fe^{III}\ (\text{low-spin}),\ Co^{III}\ (\text{low-spin}) \qquad (3)$$

by spectroelectrochemistry and EPR spectroscopy. In addition, complexes **3** and **3′** each display a reversible metal-centered reduction wave at −1.19 V, whereas for **5** and **5a** this one-electron reduction is irreversible[11] ($E_{p,red} \sim -1.0$ V). Che et al.[12] reported the first reversible oxidation and the metal-centered one-electron reduction for the series of low-spin complexes *trans*-$[Fe^{III}(bpc)X_2]^+$ (X = PBu_3, imidazole, 1-methylimidazole, ^{tert}butylpyridine, pyridine), but they did not report the second oxidation wave at a very positive potential.

The cyclic voltammograms of complexes **6** and **7** are very similar. Both each exhibit two overlapping one-electron oxidation waves at $E^1_{1/2} = +0.53$ and $+0.61$ V and $E^2_{1/2} = +0.40$ and $+0.47$ V, respectively. In addition, they are each reversibly (or quasi-reversibly) reduced by one electron at −1.32 and −1.10 V. We assign these processes as depicted in eq 4 for **6**

$$[\{Fe^{IV}(bpb^{ox1})(CN)\}_2(\mu\text{-}N)]^+ \underset{+e}{\overset{-e}{\leftrightarrows}} [\{Fe^{IV}(bpp)(CN)\}(\mu\text{-}N)Fe^{IV}(bpb^{ox1})(CN)]^0 \underset{+e}{\overset{-e}{\leftrightarrows}}$$

$$[\{Fe^{IV}(bpb)(CN)\}_2(\mu\text{-}N)]^- \underset{+e}{\overset{-e}{\leftrightarrows}} [\{Fe^{III}(bpb)(CN)\}(\mu\text{-}N)\{Fe^{IV}(bpb)(CN)\}]^{2-} \qquad (4)$$

and analogously for **7** involving $(bpc^{ox1})^-$. Thus the two $(bpb)^{2-}$ ligands in **6** and **7** are successively one-electron-oxidized, yielding one and then two $(bpb^{ox1})^-$ ligands. One-electron reduction of **6** and **7** produces the corresponding mixed-valent species containing a $[Fe^{III}(\mu\text{-}N)Fe^{IV}]^{4+}$ core and two $(bpb)^{2-}$ ligands. The cyclic voltammogram of **7a** displays two irreversible oxidations but two reversible, metal-centered one-electron reduction waves. Thus, the $[\{Fe^{III}(bpc)(N_3)\}_2(\mu\text{-}N)]^{3-}$ oxidation level is electrochemically accessible at very negative potentials.

Since the electrochemically generated (−40 °C), monooxidized species of complexes **3′**, **5**, and **5a**, namely, $[Fe^{III}(bpb^{ox1})(CN)_2]^0$ (**4**), $[Co^{III}(bpb^{ox1})(CN)_2]^0$, and $[Co^{III}(bpc^{ox1})(CN)_2]^0$, are stable in CH_3CN solution, we recorded their UV−vis spectra. As was reported previously[11,12] for $[Fe^{III}(bpc^{ox1})(PBu_3)]^{2+}$ and $[Co^{III}(bpb^{ox1})(CH_3)(H_2O)]^+$, the spectra display intense new absorptions in the visible and near-infrared regions that are characteristic of the radical of 1,2-diaminobenzene. From these data, it is clear that ligand-rather than metal-centered one-electron oxidations are observed in these cases.

The X-band EPR spectrum of **2** in frozen acetonitrile at 10 K displays a typical high-spin ferric ($S = {}^5/_2$) signal with $g \sim 4.5$ and a very weak signal at $g \sim 2.0$. A similar spectrum has been reported for $[Et_4N][Fe(bpc)(CH_3CO_2)_2]\cdot CHCl_3$.[10]

In contrast, the X-band EPR spectrum of **3′** in frozen acetonitrile at 10 K displays a rhombic signal with $g_x = 2.242$, $g_y = 2.208$, and $g_z = 1.949$, in agreement with its $S = {}^1/_2$ ground state. A very similar spectrum has been reported for $[Fe^{III}(bpb)(py)_2]ClO_4$[10] at 77 K ($g_1 = 2.258$, $g_2 = 2.182$, $g_3 = 1.943$). When **3** dissolved in an acetone/CH_2Cl_2 mixture (1:1) was electrochemically oxidized by one electron at −45 °C, the resulting solution containing **4** was EPR silent, in excellent agreement with the diamagnetic properties of **4** ($S = 0$). When the same solution was further oxidized by another electron, at a higher potential (1.7 V), $[Fe^{III}(bpb^{ox2})(CN)_2]^+$ was generated and displayed an axial EPR signal at $g_x = g_y = 2.211$, and $g_z = 1.961$, typical for a low-spin ferric complex. This behavior clearly indicates that both oxidations of **3′** are ligand-centered. The diamagnetic ground state of **4** is achieved via strong intramolecular antiferromagnetic coupling between a low-spin ferric ion and the ligand radical $(bpb^{ox1})^-$.

We also recorded the X-band EPR spectra of $[Co^{III}(bpb^{ox1})(CN)_2]^0$ and $[Co^{III}(bpc^{ox1})(CN)_2]^0$, which were both generated electrochemically at −40 °C in acetonitrile solution. The room-temperature spectra and that recorded at 60 K of both complexes are shown in Figures S2−S4 (Supporting Information). The X-band spectrum of $[Co^{III}(bpb^{ox1})(CN)_2]$ at 295 K in CH_3CN consists of a complex multiline pattern centered at $g = 2.019$ with well-resolved hyperfine splitting to the ^{59}Co nucleus ($a_{Co} = 1.53$ mT), two equivalent nitrogen atoms ($a_N = 0.328$ mT), and two equivalent hydrogens ($a_H = 0.367$ mT). It was simulated with a Lorentzian line width of 0.16 mT. We assign this signal to a cobalt(III)-coordinated ligand radical, $(bpb^{ox})^-$, with $S = {}^1/_2$. In addition, we observe a second unresolved signal at $g = 2.021$, which is probably due to decomposition of $[Co(bpb^{ox1})(CN)_2]$ at room temperature. This signal is absent for preparations at −40 °C whose EPR spectra were recorded immediately after cooling to 10 K.

The EPR spectrum of $[Co(bpc^{ox1})(CN)_2]$ in CH_3CN at 295 K (Figure S3) consists of a signal at $g = 2.006$ which displays hyperfine splitting to the ^{59}Co center ($a_{Co} = 1.53$ mT) and to two equivalent nitrogens ($a_N = 0.37$ mT) (line width 0.26 mT). The spectrum recorded at 10 K is identical to that of $[Co(bpb^{ox1})(CN)_2]$ at 10 K and is not shown. The above two EPR spectra of $[Co^{III}(bpb^{ox1})(CN)_2]$ and those of its $(bpc^{ox1})^-$ analogue unambiguously show that the phenylenediamine central part of the ligands $(bpb)^{2-}$ and $(bpc)^{2-}$ has undergone a one-electron oxidation, with formation of the corresponding (imino)semiquinonato radicals.

Mössbauer Spectra. Mössbauer spectra of polycrystalline samples were recorded in the temperature range 4.2−200 K and with applied fields of 0−7 T. The results are summarized in Table 4.

The zero-field Mössbauer spectra of mononuclear **1**, **2**, and **2a** at 80 K each consist of a broad, mostly unresolved doublet with isomer shifts typical for octahedral high-spin ferric ions ($\delta = 0.41$, 0.55, and 0.51 mm s^{-1}, respectively). The previously reported[10] spectrum of $[Et_4N][Fe^{III}(bpc)(CH_3CO_2)_2]$ is very similar.[22] In contrast, the spectrum of **3** displays a well-resolved, symmetrical quadrupole doublet with isomer shift and quadrupole splitting parameters characteristic of octahedral low-spin ferric ions and closely resembles that of low-spin $[Fe^{III}(bpb)(py)_2]ClO_4$.[10,22] Interestingly, the Mössbauer parameters of $[Fe^{III}(bpb^{ox1})(CN)_2]$ (**4**) displaying a well-resolved quadrupole doublet are similar to those of **3** although its isomer shift at 0.021 mm s^{-1} is slightly less positive than that of **3** at 0.085 mm s^{-1}. The quadrupole splitting, ΔE_Q, increases from 1.38 mm s^{-1} for **3** to 1.65 mm s^{-1} for **4**. These observations bolster the notion that the one-electron oxidation **3** → **4** is essentially ligand-centered rather than metal-centered.

(22) The broad asymmetric appearance of the zero-field spectra of solid **1**, **1a**, **2**, and **2a** at 80 K indicates intermediate-spin relaxation processes with relaxation rates that are comparable to the nuclear Larmor precession rate. This is often observed for solid monomeric high-spin iron(III) complexes because spin−lattice relaxation is mostly ineffective in these cases due to the vanishing orbital momentum of the ^6S ion with the $t_{2g}{}^3e_g{}^2$ electron configuration. The relaxation rates are then determined by temperature-independent spin−spin relaxation processes that arise from weak intermolecular spin couplings in the solid. The Mössbauer lines of **3** and **3′** are narrow because of fast spin relaxation, presumably due to fast spin−lattice relaxation which is mediated by a stronger orbital moment of the low-spin ions with the $t_{2g}{}^5$ configuration.

Table 4. Zero-Field Mössbauer Data at 80 K

complex	S^a	δ,^{b} mm s^{-1}	ΔE_Q,^{c} mm s^{-1}	Γ, mm s^{-1}	ref
1	$^5/_2$	0.41	0.92	0.97	this work
2	$^5/_2$	0.55	*d*		
2a	$^5/_2$	0.51	*d*		
3	$^1/_2$	0.085	1.38	0.33	
4	0	0.021	1.65	0.45	
6	0	−0.12	0.63	0.33	
7	0	−0.10	1.41	0.42	
7a	0	−0.09	1.28	0.33	
$[Fe^{III}(bpb)(py)_2]ClO_4$	$^1/_2$	0.12	2.36^e		10
$[Et_4N][Fe^{III}(bpc)(CH_3CO_2)_2]$	$^5/_2$	0.45	0.82^e		10
$[Fe^{III}_2(\mu\text{-}O)(bpc)_2(DMF)]\cdot 2H_2O$	0	0.49	1.48^f		13

^{a} Ground state. ^{b} Isomer shift vs α-Fe at 295 K. ^{c} Quadrupole splitting. ^{d} Broad unresolved doublet. ^{e} 77 K. ^{f} 300 K.

The zero-field spectra of dinuclear **6**, **7**, and **7a** each display a single quadrupole doublet. The isomer shift is negative in the narrow range −0.09 to −0.12 mm s^{-1}. This indicates the presence of low-spin iron(IV) ions ($S = 1$), which renders the oxidation level of the tetradentate ligands (bpb)$^{2-}$ and (bpc)$^{2-}$.

Photolyses of 2 at 77 K. Photolysis of **2** in frozen deaerated acetone with 250 nm light at 77 K was performed as described in the Experimental Section. The resulting frozen sample was immediately transferred, in two parts, to a Mössbauer and an EPR spectrometer. The zero-field Mössbauer spectrum showed that ∼40% starting material **2** was still present, in addition to one product with isomer shift and quadrupole splitting parameters of 0.07 mm s^{-1} and 1.26 mm s^{-1}, respectively, which are very similar to those observed for **3**—an octahedral low-spin ferric complex. Thus, photolysis of **2** in frozen solution does *not* produce nitridoiron(V), or a ferrous species. Instead, we propose that the low-spin species $[Fe^{III}(bpb^{ox2})(N)(N_3)]^-$ is produced. The EPR spectrum of the same frozen sample recorded at 10 K shows the signal of **2** at $g \sim 4.3$ and a complex line pattern in the low-spin region which could be deconvoluted into three subspectra (a, b, c) as shown in Figure 3. The strong component, subspectrum a, with the prominent derivative lines at $g = 2.3$ and 2.2 apparently originates not from the primary photolysis product of **2** but from a deterioration product in the sample, since the same species is practically exclusively observed after thawing the photolyzed sample for 2 min, as shown in Figure 4. For the original sample, this subspectrum accounts for 19% of the total integral intensity (including the $S = {}^5/_2$ signals of the starting material at $g = 4.3$ and $g \approx 9$, not shown in Figure 3). Another prominent, but very narrow, derivative line with weak integral intensity (1%) is found in the isotropic signal at $g = 2.007$. We attribute this component, subspectrum b, to traces of "free" radicals in the sample. Hence, the primary photoproduct of **2** is represented by the major component, subspectrum c, which accounts for 60% of the total spectral intensity. It can be simulated with rhombic g values: $\bar{g} = (1.90, 1.85, 1.48)$. In conjunction with the magnetic Mössbauer spectra discussed below, the primary photoproduct can be identified as a low-spin ferric iron species.

Since the average g values of subspectrum c deviate considerably from the free-electron value ($\sum g_i^2 = 9.22$), one might question the interpretation of low-spin iron(III) with a strong spin−orbit interaction. On the other hand, it is well-known that, in oxo(porphyrinato)iron(IV) cation-radical complexes, competing antiferromagnetic exchange and zero-field interactions (ZFS) of Fe(IV) ($S = 1$) and the ligand radical ($S' = {}^1/_2$) may lead to unusually low g values[23,24] due to mixing of the total spin $S_t = {}^1/_2$ and $S_t = {}^3/_2$ multiplets. We therefore explored the possibility that photolyzed **2** might be an Fe(IV) complex with a ligand radical, where the spin ground state of $S_t = {}^1/_2$ owes its origin to antiferromagnetic spin coupling between a low-spin Fe^{IV} ion ($S = 1$) and the radical ($S' = {}^1/_2$). In fact, an intriguingly good

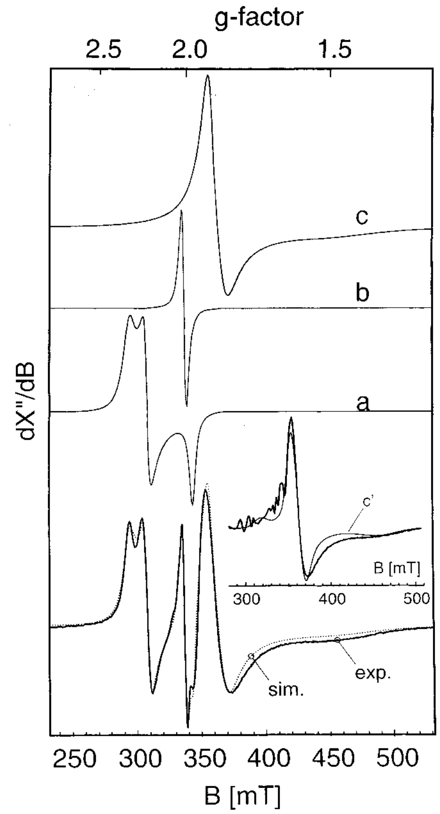

Figure 3. X-band EPR spectrum and simulations of the low-temperature photolyzed complex **2** in CH_3CN at 10 K. Experimental conditions: microwave frequency 9.4671 GHz, microwave power 50 μW, modulation amplitude 3 mT. Subspectra a−c are simulations with effective g values and angular-dependent line widths and Lorentzian line shapes: (a) $\bar{g} = (2.302, 2.196, 1.968)$, $W = (13.3, 7.4, 7.0)$ mT; (b) isotropic $g = 2.007$, $W = 7.8$ mT; (c) $\bar{g} = (1.895, 1.846, 1.48)$, W = (12.9, 20.9, 11.4) mT. Inset: experimental spectrum without subspectra a and b (subtracted, bold line) and a spin-Hamiltonian simulation for Fe(IV), $S = 1$, and a radical, $S' = {}^1/_2$ (subspectrum c′, thin line). For Fe(IV), $D = 16.4$ cm^{-1}, $E/D = 0.33$, and $\bar{g} = (2.092, 2.19, 1.996)$, where $\bar{g}$ is calculated from D and E/D by using a ligand field model[24] and a spin−orbit coupling constant $\zeta = 500$ cm^{-1}. For the radical, $g = 2.002$. Isotropic and anisotropic contributions to the exchange coupling tensor: $J^{iso} = -10$ cm^{-1}; $J^{aniso} = (-2, 0.95, 1.05)$ cm^{-1}.

(23) Rutter, R.; Hager, L. P.; Dhonau, H.; Hendrich, M.; Valentine, M.; Debrunner, P. G. *Biochemistry* **1984**, *23*, 6809.

(24) (a) Oosterhuis, W. T. *J. Chem. Phys.* **1973**, *58*, 4757. (b) Paulsen, H.; Müther, M.; Grodzicki, M.; Tautwein, A. X.; Bill, E. *Bull. Soc. Chim Fr.* **1996**, *133*, 703.

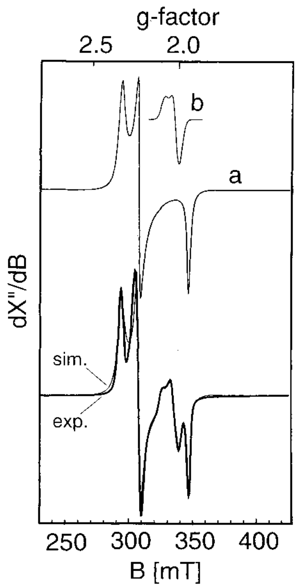

Figure 4. X-band EPR spectrum of the photolyzed sample at 10 K after thawing for 2 min. The subspectra are simulations with effective g values and angular-dependent line widths: (a) $\bar{g}$ = (2.303, 2.197, 1.950), W = (6.9, 3.6, 3.8) mT (Gaussian, 97% intensity); (b) $\bar{g}$ = (2.070, 2.015, 1.994), W = (7, 8, 7) mT (Gaussian, 3% intensity).

representation of subspectrum c was obtained from a spin-Hamiltonian simulation if the ratio of exchange and ZFS parameters, $|2J|/D$, was about 1.25. This alternative result is shown in the inset of Figure 3 for comparison with the experimental spectrum from which subspectra a and b were subtracted. This interpretation, however, was spectroscopically refuted for the following reasons. First, we did not observe experimental evidence for the presence of an excited spin quartet state ($S_t = {}^3/_2$), which for reasonable values of $D \leq 20$ cm^{-1} (and the corresponding J values) should be found at energies of less than 30 cm^{-1} (43 K). Second, if $D \leq 20$ cm^{-1}, the antiferromagnetic coupling between the Fe^{IV} ion and the ligand radical must be of the order of $|J| \sim 20$ cm^{-1}, which is too small, considering the experimentally verified strong coupling in room-temperature diamagnetic **4**. In conjunction with the following magnetic Mössbauer measurements, the hypothesis of an Fe(IV)−radical system for photoproduct of **2** was discarded.

Applied field Mössbauer spectra of the low-temperature photolyzed complex **2** (35% enriched with ^{57}Fe) were recorded at liquid helium temperatures with fields in the range 1−7 T. They showed a superposition of well-resolved magnetic hyperfine patterns of a "low-spin" component with small overall splitting of about 6 mm s^{-1} and of a "high-spin" component with large overall splitting of about 16 mm s^{-1}. The latter was unambiguously assigned to the ferric starting material **2**, and to facilitate simulations of the photoproduct spectrum, its contribution (∼35%) was stripped-off from the data by using experimental spectra of **2** that were recorded under the same conditions.

The difference Mössbauer spectra of photolyzed **2** at various fields are shown in Figure 5. They were simulated by adopting a single $S = {}^1/_2$ species with isomer shift and quadrupole splitting parameters taken from the zero-field spectra and the g values (1.90, 1.85, 1.48) determined by EPR spectroscopy. From a systematic search in the parameter space of the spin-Hamiltonian, we obtained the best solution for the magnetic hyperfine tensor at $\bar{A}/g_N\beta_N$ = (−33.4, −16.55, +0.54) T, in conjunction with the large asymmetry parameter $\eta = 0.95$. The electric field gradient (efg) tensor shows significant Euler

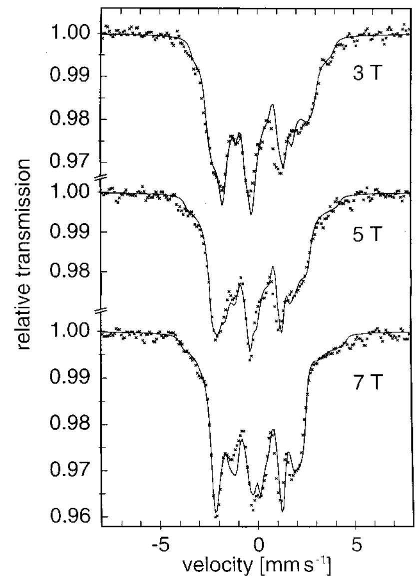

Figure 5. Applied field Mössbauer spectra of low-temperature photolyzed **2** measured at 3, 5, and 7 T perpendicular to the γ-rays and at 4.2 K. A ferric high-spin contribution of 35% relative intensity from starting material **2** was subtracted from each of the experimental spectra. The solid lines are spin-Hamiltonian simulations for low-spin Fe(III) ($S = {}^1/_2$) as described in the text.

rotations of $\alpha = 46°$, $\beta = 82°$, and $\gamma = 102°$ with respect to the **g** and **A** tensors. Both features, the anisotropic **A** tensor and the large, asymmetric, and rotated efg tensor, are quite consistent with expectations for low-spin Fe^{III} with strong spin−orbit mixing of 3d levels due to the electron hole in the t_{2g} orbital manifold.[1,25,26]

The alternative interpretation of the electronic structure of photolyzed **2**, namely, the presence of Fe(IV) and a spin-coupled ligand radical, could be definitively excluded from the corresponding simulations of the magnetic Mössbauer spectra. It turned out that, under the condition $|2J|/D \approx 1.25$ required to explain the EPR spectra, the spin ground doublet "$S_t = {}^1/_2$" is characteristically perturbed by mixing with excited states if strong fields are applied. The resulting field dependence of the simulated Mössbauer spectra, however, was not compatible with the experimental data. In particular, the behavior of the overall splitting and the shoulders at +4/−4 mm s^{-1} observed in the 7 T spectrum could not be reproduced in the spin-coupling model.

We mention that the decomposition product, whose signals were observed in the EPR spectra of Figures 3 and 4 (subspectrum a), was not found in sizable amounts in the Mössbauer sample of photolyzed **2**. We assume that this is due to a difference in the preparations of the Mössbauer cups and of the EPR tubes. After the sample transfer under liquid nitrogen, the EPR quartz tubes, in contrast to the Mössbauer cups, had to be purged of the residual coolant by gentle pumping. We cannot exclude the possibility that the EPR sample might have been slightly warmed during this procedure to about 100 K for a few minutes.

(25) (a) Griffith, J. S. *Proc. R. Soc. London, Ser. A* **1956**, *235*, 23. (b) Oosterhuis, W. T.; Lang, G. *Phys. Rev.* **1969**, *178*, 439−456. (c) Taylor, C. P. S. *Biochem. Biophys. Acta* **1977**, *491*, 137. (d) Huynh, B. H.; Emptage, M. H.; Münck, E. *Biochim. Biophys. Acta* **1978**, *534*, 295−306.

(26) (a) Walker, F. A.; Huynh, B. H.; Scheidt, W. R.; Osvath, S. R. *J. Am. Chem. Soc.* **1986**, *108*, 5288−5297. (b) Walker, F. A.; Nasri, H.; Turowska-Tyrk, I.; Mohanrao, K.; Watson, C. T.; Shokhirev, N. V.; Debrunner, P. G.; Scheidt, W. R. *J. Am. Chem. Soc.* **1996**, *118*, 12109−12118.

Scheme 1

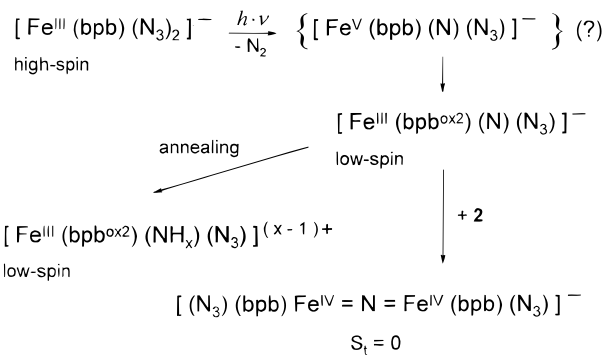

Discussion

The investigation of the mononuclear dicyanometal complexes **3**, **3′**, **5**, and **5a** has unambiguously established that they contain a low-spin ferric or a low-spin cobalt(III) ion and a $(bpb)^{2-}$ or $(bpc)^{2-}$ ligand. Their one- and two-electron oxidation products have been shown to be species that also contain a low-spin ferric or cobalt(III) ion and the radical anion $(bpb^{ox1})^-$ or $(bpc^{ox1})^-$ or the diamagnetic ligand $(bpb^{ox2})^0$ or $(bpc^{ox2})^0$. In diamagnetic **4**, the observed singlet ground state is attained via a strong, intramolecular antiferromagnetic coupling between a low-spin ferric ion (d^5, $S = {}^1/_2$) and a $(bpb^{ox1})^-$ ligand radical ($S = {}^1/_2$). It is important to note that the 80 K Mössbauer ^{57}Fe isomer shift values, δ, of **3** and **4** at 0.085 and 0.021 mm s^{-1} are similar.

In contrast, in **6**, **7**, and **7a**, low-spin Fe^{IV} ions ($S = 1$) are present, and consequently, the isomer shift parameters are observed at ~ -0.10 mm s^{-1}, which represents a shift of ~ 0.15 mm s^{-1} for a one-electron change in the oxidation state. This is typical for octahedral complexes containing low-spin ferric and Fe^{IV} ions in similar ligand environments and has been reported for a series of low-spin *trans*-[(cyclam)FeX_2] complexes containing Fe^{II}, Fe^{III}, Fe^{IV}, and even Fe^V. The isomer shift varies linearly with the formal oxidation state of the iron ion (~ 0.15 mm s^{-1} shift per one-electron change in oxidation number).[1] Using such a correlation in the present case, one would predict an isomer shift of $\sim -0.3 \pm 0.1$ mm s^{-1} for a genuine nitridoiron(V) species with a $(bpb)^{2-}$ or $(bpc)^{2-}$ ligand. We have not found experimental evidence for the occurrence of such a species.

It is therefore significant that the primary photolysis product of **2** displays an isomer shift at 77 K of 0.07 mm s^{-1}, thereby indicating the presence of a low-spin ferric ion rather than a higher oxidation state iron in (Fe^{IV} or Fe^V). In conjunction with its EPR spectrum confirming the expected $S = {}^1/_2$ ground state, we propose the reaction sequence shown in Scheme 1 yielding a very reactive nitridoiron(III) species for the photolysis of **2** at cryogenic temperatures. The photolytic cleavage of one N−N bond in a coordinated azido ligand in **2** probably yields dinitrogen and a very oxidizing nitridoiron(V) transient intermediate that is transformed via an intramolecular two-electron transfer from the $(bpp)^{2-}$ ligand to the first spectroscopically detectable photolysis product, namely, low-spin $[Fe^{III}(bpb^{ox2})(N)(N_3)]^-$. Since the nitrido ligand cannot be stabilized via π-donor back-bonding to iron(III) to the same extent as, e.g., in $V^V{\equiv}N$ (d^0), $Cr^V{\equiv}N$ (d^1), or $Mn^V{\equiv}N$ (d^2) complexes because the t_{2g} level is already filled with five electrons, the nitride in this intermediate is very nucleophilic (basic) indeed. Upon annealing of the frozen sample, it will probably be immediately protonated, forming an imide, amide, or ammonia ligand. One of these species is thought to be the source of the EPR signal described above (subspectrum a in Figure 3).

On the other hand, if the starting complex **2** is present in large excess over the first photolysis product (which is the case when **2** is photolyzed in solution at ambient temperature), this species will react in a bimolecular fashion with **2**, generating the dinuclear complex **7**. The absence of photochemically generated ferrous ions explains why no mixed-valent complexes containing the $[Fe^{III}{=}N{=}Fe^{IV}]^{4+}$ core have been detected.

After submission of this paper, a report by Mukherjee et al.[27] appeared describing the synthesis and characterization of diamagnetic $[Fe^{III}(bpb^{ox1})(CN)_2]$. Where our data overlap with theirs, agreement is excellent; in particular, their Mössbauer data are identical with those reported here.

In another recent paper, by Scheidt et al.,[28] the synthesis and crystal structure are described for $\{[Fe(TTP)]_2N\}SbCl_6$, containing an $[Fe^{IV}{=}N{=}Fe^{IV}]^{5+}$ core (TTP = tetratolylporphinate). The $Fe{-}N_b$ bond distance is very short at 1.6280(7) Å. In contrast to complexes **6** and **7**, the iron(IV) ions are five-coordinate.

Acknowledgment. S.D. thanks the Alexander von Humboldt Foundation for a stipend, and we all thank the Fonds der Chemischen Inustrie for financial support.

Supporting Information Available: Figures S1 (cyclic voltammogram of **3**), S2 (X-band EPR spectrum and its simulation of $[Co^{III}(bpb^{ox1})(CN)_2]$ at 295 K), S3 (X-band EPR spectrum and its simulation of $[Co^{III}(bpc^{ox1})(CN)_2]$ at 295 K), and S4 (X-band EPR spectrum and its simulation of $[Co^{III}(bpb^{ox1})(CN)_2]$ at 60 K), Tables S1−S25 (crystallographic and structure refinement data, atom coordinates, bond lengths and angles, anisotropic thermal parameters, and calculated positional parameters of H atoms for **2**, **3**, **5a**, **6**, and **7**), Table S26 (bond distances of the carboxamide units in the complexes), Table S27 (infrared spectroscopic data for the complexes), Table S28 (electronic spectral data for the complexes), and X-ray crystallographic files, in CIF format, for **2**, **3**, **5a**, **6**, and **7**. This material is available free of charge via the Internet at http://pubs.acs.org.

IC0001107

(27) Patra, A. K.; Ray, M.; Mukherjee, R. *Inorg. Chem.* **2000**, *39*, 652.
(28) Li, M.; Shang, M.; Ehlinger, N.; Schulz, C. E.; Scheidt, W. R. *Inorg. Chem.* **2000**, *39*, 580.